2018

Structural, magnetic, and electron-transport properties of epitaxial Mn_2PtSn films

Y. Jin

Shah R. Valloppilly

Parashu Kharel

Jace Waybright

Pavel V. Lukashev

See next page for additional authors

Authors

Y. Jin, Shah R. Valloppilly, Parashu Kharel, Jace Waybright, Pavel V. Lukashev, Xingzhong Li, and David J. Sellmyer

Structural, magnetic, and electron-transport properties of epitaxial Mn_2PtSn films

Y. Jin,[1,2] S. Valloppilly,[2] P. Kharel,[2,3,a)] J. Waybright,[3] P. Lukashev,[4] X. Z. Li,[2] and D. J. Sellmyer[1,2,b)]
[1]*Department of Physics and Astronomy, University of Nebraska, Lincoln, Nebraska 68588, USA*
[2]*Nebraska Center for Materials and Nanoscience, University of Nebraska, Lincoln, Nebraska 68588, USA*
[3]*Department of Physics, South Dakota State University, Brookings, South Dakota 57007, USA*
[4]*Department of Physics, University of Northern Iowa, Cedar Falls, Iowa 50614, USA*

(Received 22 June 2018; accepted 24 August 2018; published online 12 September 2018)

The growth of new magnetic materials on suitable insulating substrates is an important part of the development of spin-electronics devices for memory or information processing. Epitaxial thin films of Mn_2PtSn were grown on a MgO [001] substrate by magnetron co-sputtering of the constituents. Structural, magnetic, and electron-transport properties were investigated. The epitaxial Mn_2PtSn film has an inverse tetragonal structure with the c-axis aligned in the plane of the MgO substrate. The lattice constants determined using XRD and TEM analysis are $c = 6.124$ Å and $a = b = 4.505$ Å. The orientation of Mn_2PtSn c-axis which is 45° away from the a-axis of MgO has resulted in a small lattice mismatch of about 2.8%. The measured saturation magnetization is 5.3 μ_B/f.u., which is smaller than the first-principles calculated value of 6.4 μ_B/f.u. for ferromagnetic spin arrangement. Magnetization measurements determined the bulk magnetocrystalline anisotropy constant K_v of about 11.3 Merg/cm^3 (1.13 MJ/m^3). The electron-transport behavior is similar to that of normal magnetic metals. These results indicate that Mn_2PtSn may have promising applications in spintronic devices. *Published by AIP Publishing.* https://doi.org/10.1063/1.5045667

I. INTRODUCTION

In recent years, there have been extensive efforts in developing new materials that are suitable for spin-transport-based devices including one of the most promising nonvolatile memory technologies, namely, the spin-transfer-torque (STT)-based magnetic random-access memory (MRAM).[1–8] Similarly, materials with non-collinear magnetic texture, e.g., magnetic skyrmions have attracted much interest in memory or other applications.[9–11] Heusler compounds are favorable for spintronics due to their high Curie temperature (T_c) and high spin polarization, and the family of tetragonal Heusler compounds exhibits anisotropic magnetic structures. Some of the Mn-based Heusler compounds are such materials with a tetragonal structure, uniaxial magnetic anisotropy, high T_c, relatively low saturation magnetization (M_s), and a high degree of spin polarization (P).[6,12] The most prominent examples are $Mn_{3-x}Ga$,[13] $Mn_{3-x}Co_xGa$,[6,14] Mn_3Ge,[15] Mn_2PtIn,[16] and Mn_2RhSn.[6–8,14–20] Mn_2PtSn is theoretically predicted to have an inverse tetragonal crystal structure, high P, and large magnetocrystalline anisotropy (MCA) of about 3.04 meV (50 Merg/cm^3).[6,21] However, the MCA in the inverse tetragonal Mn_2PtSn alloy prepared using melt spinning and annealing has been found to be 4.9 Merg/cm^3 at 5 K,[22,23] which is about one order of magnitude smaller than the theoretically predicted value; this may be due to a non-collinear spin structure similar to that found in Mn_2RhSn compounds.[20]

Recently, the observation of the room-temperature magnetic anti-skyrmion structure by the Lorentz transmission electron microscope and giant topological Hall effect in the Mn-Pt-Sn system was reported, which also points to the possible non-collinear spin structure in Mn-Pt-Sn alloys.[9,10] The potential application in devices and the interesting spin structure in Mn_2PtSn compounds motivated us to undertake a comprehensive study on single-phase epitaxial thin films of Mn_2PtSn. Additionally, the prospective materials need to be grown as epitaxial thin films on MgO, a commonly used tunneling barrier, since magnetic-tunnel-junctions (MTJ) are the main memory elements of STT memory devices. Here, we report a structural, magnetic, and electron-transport study on single-phase epitaxial thin films of Mn_2PtSn. The film growth, orientation, magnetization, magnetic anisotropy, and transport properties are discussed.

II. EXPERIMENTAL METHODS

All investigated Mn_2PtSn films were deposited on atomically flat MgO [001] using a magnetron sputtering system with a base pressure of about 3×10^{-8} Torr. The films were prepared by co-sputtering Mn, Pt, and Sn targets under optimized conditions for which the Ar sputtering pressure of 2×10^{-3} Torr and the substrate temperature of 773 K were used. A DC power source of 52.5 W was used to sputter Mn, whereas Pt and Sn were sputtered with the help of 10.0 W and 26.4 W RF power sources, respectively. The crystal structure of the films and the epitaxial relationship between Mn_2PtSn and MgO were investigated using a Rigaku SmartLab Diffractometer and a Bruker-AXS D8 Discover Diffractometer with Cu Kα radiation (wavelength of 1.5406 Å) and a FEI Tecnai Osiris (Scanning) Transmission Electron Microscope (TEM). The electron diffraction simulation was carried out

a)parashu.kharel@sdstate.edu
b)dsellmyer@unl.edu

using Landyne software suite.[23] The elemental compositions of the samples were determined using energy-dispersive x-ray spectroscopy (EDX) in a FEI Nova NanoSEM450. The magnetic and electron-transport properties were measured using a Quantum Design SQUID magnetometer (MPMS) and a physical property measurement system (PPMS).

III. RESULTS AND DISCUSSION

Figure 1 shows the out-of-plane XRD pattern (gray line plot) and several asymmetric Bragg reflections (colored, partial scans) of the epitaxial Mn_2PtSn film prepared on a MgO [001] substrate. The two strong peaks around 43° and 94° are from the MgO substrate, and the other two prominent peaks around 28° and 58° are from the Mn_2PtSn film. In our previous work on bulk Mn_2PtSn,[23] we have shown that Mn_2PtSn crystallizes in the inverse tetragonal structure with space group I-4m2 (SG # 119) and lattice parameters $a = b = 4.512$ Å and $c = 6.084$ Å. In this structure, Mn atoms occupy the 2b (0, 0, 1/2) and 2c (0, 1/2, 1/4) lattice sites, and Pt and Sn atoms, respectively, occupy the 2d (0, 1/2, 3/4) and 2a (0, 0, 0) sites. Based on this structure, the two prominent peaks around 28° and 58° can be attributed to the reflections from (110) and (220) planes of Mn_2PtSn, respectively. This indicates that the films are grown with a high degree of orientational relationship with the cube axes of MgO and the [110] axis is aligned along the surface normal of the MgO [001].

In order to investigate the single-crystalline properties and structure of the films, we have collected additional Bragg reflections by asymmetric x-ray reflection, grazing-incidence in-plane diffraction experiments, and pole-figure analysis. Scans performed in the off-normal angles (χ) with respect to the surface normal are useful to probe crystallographic planes away from [110] and are essential for the determination of unit cell parameters. Some of these planes accessible for Bragg scattering using the 2D diffraction method are (011), (020), (112), and (132) with their interplanar angles with respect to surface normal $\chi \sim 55°$, 45°, 46°, and 36°, respectively. The two prominent reflections (020) and (112) are adjacent to each other in both 2θ and χ, and therefore could be captured in a single frame using the 2D area detector Vantec 500 of the Bruker D8 Discover diffractometer. The 2D diffraction frame as well as the line-intensity profile extracted from the image is shown in Fig. 2. The diffraction image of Fig. 2 shows two distinct diffraction spots with slightly different intensities and χ values, which confirms the single-crystalline nature of the sample with the tetragonal unit cell as proposed above. The intensity plots extracted from diffraction images corresponding to (011), (020), (112), and (132) Bragg reflections are compiled in Fig. 1. An analysis of all these Bragg reflection peaks indicates that the unit cell parameters are $a = b = 4.505$ Å and $c = 6.124$ Å, which are very close to previously reported bulk values.[21]

Examination of the lattice parameter a for the film and the substrate ($a_{\text{film}} = 4.505$ Å and $a_{substrate} = 4.211$ Å) suggests that a large lattice strain (~7% mismatch) would exist if the film were to grow with its a-axis parallel to that of the substrate. However, our XRD data, as discussed above, show that the [110] is the surface normal and the c-axis must lie in the plane of the substrate, as these two axes are mutually orthogonal. If the c-axis is oriented at 45° away from the MgO a-axis so that the Mn_2PtSn [001] axis is parallel to MgO [110], the lattice mismatch is then reduced to ~2.8%, as depicted in Fig. 3. This orientation relationship is most likely needed for the growth of the Mn_2PtSn film on MgO and is further verified by the symmetry of the distribution of selected Bragg reflections from the pole plots and Selected Area Electron Diffraction (SAED) as discussed below.

Pole plots are ideal to confirm the high degree of crystallinity and the epitaxial relationship of the film and substrate. The pole-plots represent the 2D-representation of hemispherical

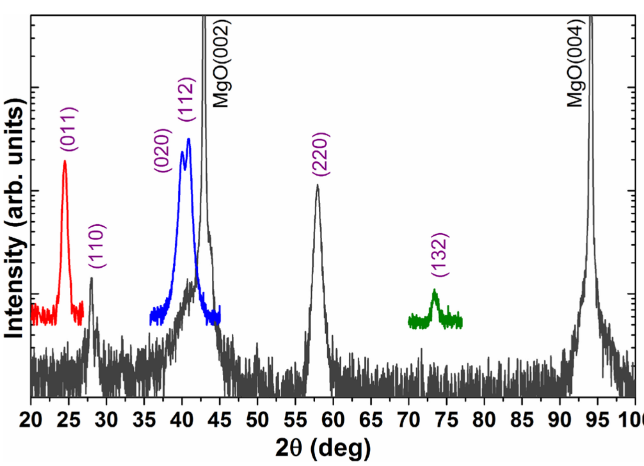

FIG. 1. Out-of-plane XRD pattern (gray line plot) and several asymmetric Bragg reflections (colored, partial scans) of the epitaxial Mn_2PtSn film prepared on the MgO(001) substrate. The partial scans obtained from Bragg reflections, off-normal to the film plane, establish the formation of the Mn_2PtSn phase in the inverse tetragonal Heusler structure.

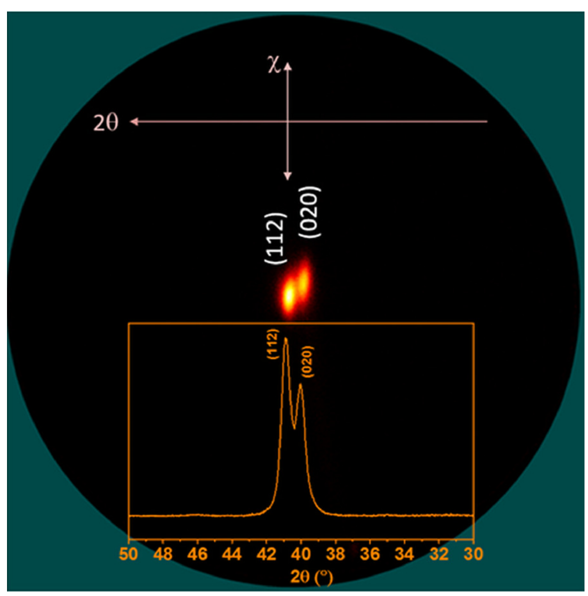

FIG. 2. The 2D diffraction frame obtained using the Vantec 500 area detector together with the intensity line profile (inset) extracted from the frame by integrating the intensity. The two axes involved in the 2D plot are 2θ and χ, as marked in the plot. The 2D diffraction image clearly demonstrates the distinct (020) and (112) Bragg reflections and their slight difference in the interplanar angles with respect to the film normal [110].

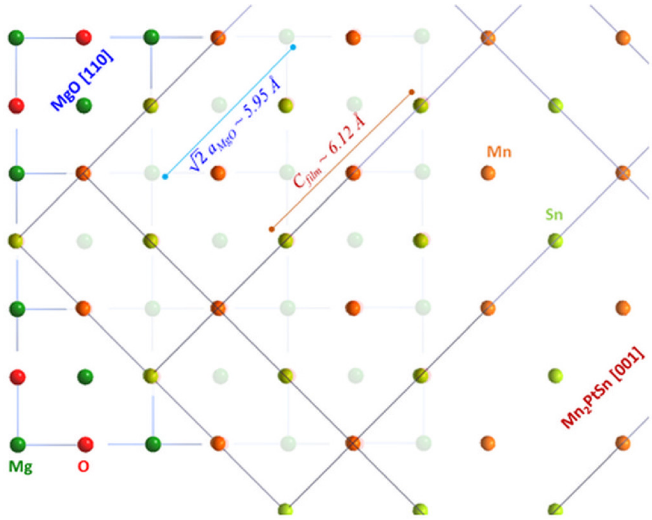

FIG. 3. Proposed lattice overlay of the Mn_2PtSn film on the MgO substrate to facilitate epitaxial growth. Here, Mn_2PtSn [110]//MgO [001] is implied along the viewing direction. The c-axis of the tetragonal inverse Heusler film is aligned with MgO [110] so that $c_{film} \sim \sqrt{2}\, a_{MgO}$.

diffraction intensity I (χ, ϕ) of a Bragg peak, where χ (0°–90°) is the inclination angle of the diffraction vector with respect to the surface normal and ϕ (0°–360°) is the azimuthal angle that the sample makes with respect to the beam direction, when the sample rotates around the surface normal. In this 2D representation, χ variation is designated radially from circumference (substrate plane, $\chi = 90°$) to the center (substrate normal, $\chi = 0°$) and ϕ variation is designated by the concentric circles whose radius is the projection of the tilt vector in the plane. Pole-plots represent the symmetry of the planes for a fixed tilt angle. As shown in Fig. 4(a), the strong diffraction spots and the corresponding diffraction peaks [Fig. 4(b)] indicate 4 equivalent {011} planes observable within the geometry of the experiment, which confirms epitaxial growth of the Mn_2PtSn film prepared on the MgO [001] substrate. The pole figure was collected at the Bragg angle $2\theta = 24.5°$.

In order to confirm the crystal structure and the epitaxial growth of Mn_2PtSn on MgO as indicated by the XRD analysis, we conducted a TEM analysis of the film. Figure 5 shows (a) the SAED pattern and (c) high-resolution TEM image of the film. The film has a uniform thickness of about 90 nm. The experimental and calculated SAED patterns, as shown in Figs. 5(a) and 5(b), include diffraction spots from both Mn_2PtSn [$1\bar{1}1$] and MgO [001] zone axes, where the MgO [100] and Mn_2PtSn [$1\bar{1}1$] are parallel and the Mn_2PtSn [001] is rotated away from MgO [100] by 45°. The SAED experiments are consistent with the XRD results. The observed lattice parameters indicate that there is a significant lattice mismatch between the ordered Mn_2PtSn film and the MgO substrate ($a = 4.21$ Å). As shown in Fig. 5(c), the epitaxial growth of Mn_2PtSn on MgO can be seen in the high-resolution TEM image of the film-MgO interface, which appears to be a thickness of about 1 nm. The elemental composition of the film was determined to be $Mn_{47.5}Pt_{25.2}Sn_{27.3}$ using energy-dispersive x-ray spectroscopy (EDX) in TEM.

Figure 6(a) shows the isothermal magnetization curves *M(H)* of the Mn_2PtSn film recorded at 5 K and 300 K with the external magnetic field being along *c*-axis [001] parallel to the film plane. Figure 6(b) shows *M(H)* of the Mn_2PtSn film recorded at 5 K and 300 K with the external magnetic field along [110] perpendicular to the film plane. The *M(H)* curves indicate that the film has an in-plane magnetic anisotropy with the in-plane-field coercivities of about 4 kOe at 5 K and 1 kOe at 300 K. Here, the easy axis of magnetization is the crystallographic *c* [001] direction which lies on the plane of the film (MgO substrate) resulting in an in-plane magnetic anisotropy. For the out-of-plane-field measurement, the coercivities are very small, namely, about 100 Oe at 5 K and 50 Oe at 300 K. The M_s determined from the low-temperature (5 K) *M(H)* loop is about 800 emu/cm^3 (5.3 μ_B/f.u.). This M_s is smaller than the value (6.7 μ_B/f.u.) predicted by density-functional calculations for inverse tetragonal Mn_2PtSn assuming a ferromagnetic arrangement of manganese moments.[21] The anisotropy field (H_a) defined as the magnetic field needed to saturate the magnetization of a uniaxial crystal in a hard direction is found to be 20 kOe from the *M(H)* curves. The effective anisotropy constant K_u calculated using the approach-to-saturation method is 9.3 Merg/cm^3. Here, the high-field data were fitted to $M = M_s\left[1 - A/H^2\right] + \chi H$ with $A = 4K_u^2/15M_s^2$.[24] The parameters M_s and χ are the spontaneous magnetization and the high-field susceptibility, respectively. The effective anisotropy constant K_u can be expressed as $K_u = K_v + K_s/t - K_{sh}$, where K_v, K_s, and K_{sh} are the bulk magnetocrystalline, interface and surface, and shape anisotropies, respectively. The shape anisotropy constant calculated using $K_{sh} = 2\pi M_s^2$ is about 2 Merg/cm^3 (0.2 MJ/m^3). Our samples are about 90 nm thick and the interface and surface anisotropy contribution is

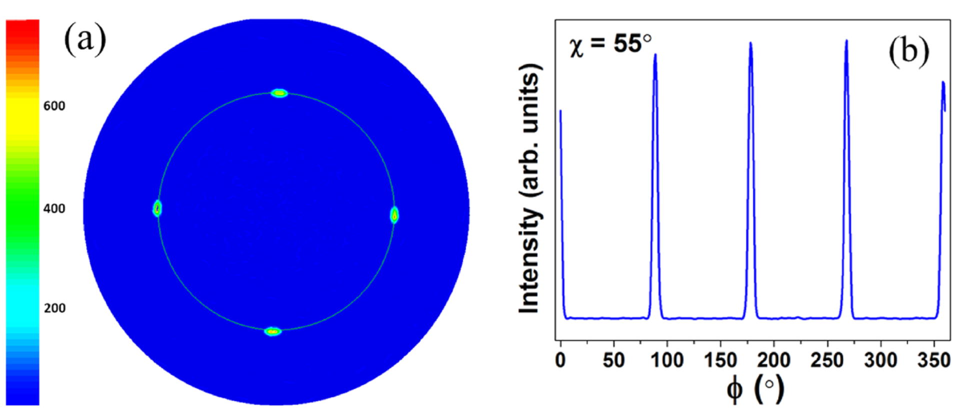

FIG. 4. (a) {011} Pole-Figure plot of Mn_2PtSn films deposited on MgO [001] and (b) ϕ-circle slice—intensity profile extracted at $\chi = 55°$. The pseudo 4-fold symmetry of the pole plot is apparent and the ϕ-circle-slice indicates the observation of equivalent (011), ($01\bar{1}$), ($10\bar{1}$), and (101) planes.

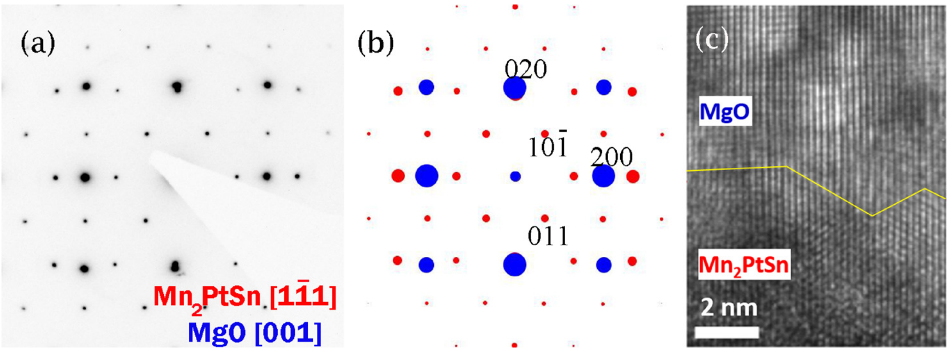

FIG. 5. TEM analysis (a) experimental and (b) calculated SAED patterns, red circles (Mn_2PtSn), blue circles (MgO), (c) high-resolution TEM image of the interface between the film and substrate.

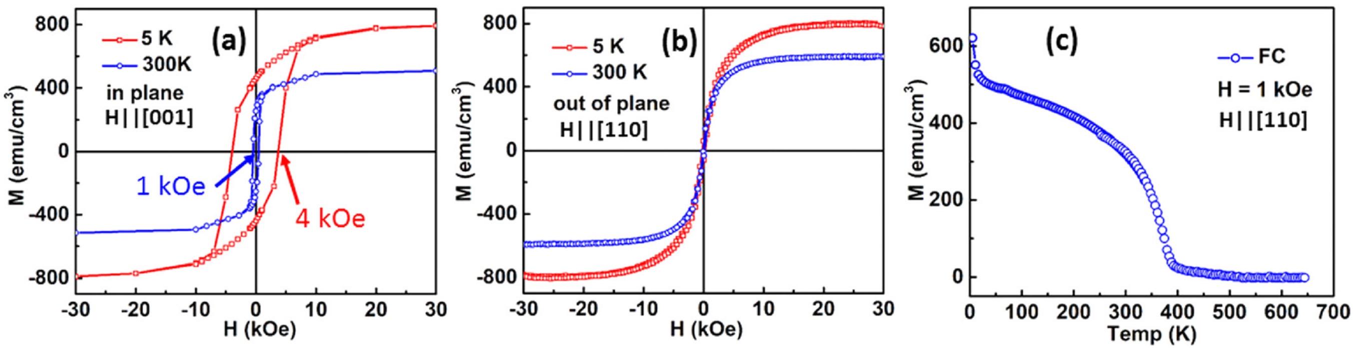

FIG. 6. Field dependence of magnetization *M(H)* loops of epitaxial Mn_2PtSn films at 5 K and 300 K with a magnetic field applied (a) in plane, and (b) perpendicular to the plane of the film. (c) Temperature dependence of magnetization of epitaxial Mn_2PtSn films with magnetic field H = 1 kOe applied out of the plane.

negligible.[25] Therefore, the bulk anisotropy constant K_v is about 11.3 Merg/cm^3 (1.13 MJ/m^3) which is considerably smaller than the theoretically predicted value of 50 Merg/cm^3,[21] based on a ferromagnetic structure. The in-plane anisotropy constant decreases as temperature increases from 5 K reaching 5.5 Merg/cm^3 at 300 K.

Figure 6(c) shows the thermomagnetic curve *M(T)* of the epitaxial Mn_2PtSn film measured at 1.0 kOe, where the magnetization shows a single magnetic transition at its Curie temperature of 380 K. The magnetostructural transition as observed in bulk Mn_2PtSn near 190 K (Refs. 10 and 21) is absent in the *M(T)* curve of our film samples. A possible reason for the lack of this transition is a result of clamping of the film to the substrate. The paramagnetic tail at low temperature may be attributed to paramagnetic nanoclusters or impurities.

Figure 7(a) shows the temperature dependence of longitudinal resistivity ρ_{xx} of the Mn_2PtSn film measured at H = 0, where the ρ_{xx} increases almost linearly as temperature increases from 30 K to 300 K, similarly to the transport behavior of normal magnetic metallic samples. The low-temperature portion of ρ_{xx} (T) below 30 K is non-linear with a residual resistivity ρ_0 of 250 $\mu\Omega$ cm. The residual resistivity ratio, ρ_{xx} (300 K)/ρ_{xx} (5 K) = 3.2, and the relatively high value of residual resistivity indicates a moderate degree of crystalline disorder in the film.

Figure 7(b) shows the magnetic field dependence of Hall resistivities $\rho_{xy}(H)$ of the Mn_2PtSn film measured at 5 K, 10 K, 30 K, and 100 K. The $\rho_{xy}(H)$ curves are nonlinear at all temperatures and look somewhat similar in shape to the corresponding *M(H)* curves. The ρ_{xy} can be expressed as $\rho_{xy}(H,T) = R_0 \cdot H + R_A \cdot M(H)$, where the first term is proportional to the external magnetic field (ordinary Hall resistivity) and the second term depends on the magnetization of the film (anomalous Hall resistivity).[26,27] R_0 and R_A in the expression are, respectively, the ordinary and anomalous Hall coefficients. These coefficients can be determined by extrapolating the high-field portion of $\rho_{xy}(H)$ curve to H = 0, where the slope and intercept of the line are equal to R_0 and R_A M(0), respectively, with M(0) being the saturation magnetization. The values of the coefficient $R_A \cdot M(H)$ derived from the plot are 0.59 $\mu\Omega$ cm, 0.55 $\mu\Omega$ cm, 0.50 $\mu\Omega$ cm, and 0.38 $\mu\Omega$ cm at temperatures 5 K, 10 K, 30 K, and 100 K, respectively. In the ρ_{xy} (H) curves of bulk Mn_2PtSn, relatively large hump-like anomalies at low H have been observed and attributed to the topological Hall effect likely originated from the emergence of chiral spin texture of magnetic skyrmions.[10] This feature is absent in our epitaxial films indicating that the spin chirality texture is not induced in the epitaxial thin film of Mn_2PtSn. Since we did not observe the structural and spin reorientation transitions near 192 K in both the *M(T)* and ρ_{xx} (T) measurements of our thin films as observed in bulk samples,[10,21] it is possible that films are clamped by the substrate suppressing the chiral spin texture.

We have determined the carrier concentration and mobility in the Mn_2PtSn films using the results of Hall measurement. The field dependence of the Hall resistivity $\rho_{xy}(H)$ of Mn_2PtSn exhibits a linear characteristic at high fields and roughly mimics the *M(H)* data. For the sake of simplicity, we have used the single-carrier band model, where $R_0 = 1/ne$ and $\mu = R_0(T)/\rho(T)$ to calculate the carrier density n and the

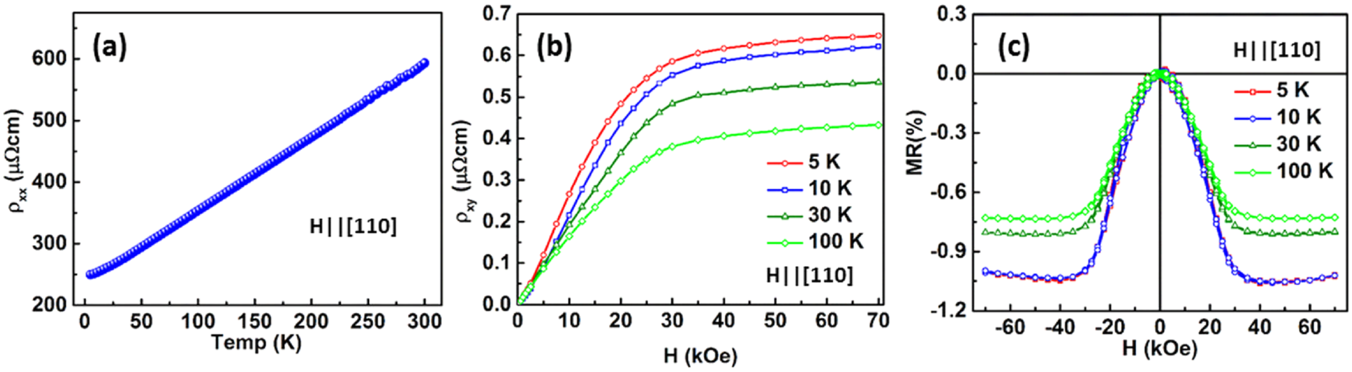

FIG. 7. (a) Longitudinal resistivity of the Mn_2PtSn film as a function of temperature with a zero magnetic field. (b) Hall resistivity of the Mn_2PtSn film measured at various temperatures with magnetic field applied perpendicular to the film plane. (c) Field dependence of magneto-resistivity (MR) of the Mn_2PtSn film for various temperatures with magnetic field applied perpendicular to the film plane.

mobility μ. Typical values of n and μ for the oriented Mn_2PtSn film at 5 K are $3.27 \times 10^{22}\,cm^{-3}$ and $30\,cm^2/(V\,s)$, respectively. The carrier concentration n of Mn_2PtSn is comparable to that of Cu ($8.5 \times 10^{22}\,cm^{-3}$) while the carrier mobility is much lower than that of Cu [$428\,cm^2/(V\,s)$]. The low carrier mobility corresponds to the low MR ratio of Mn_2PtSn as depicted in Fig. 7(c).

Figure 7(c) shows the magnetic field dependent magneto-resistivity (MR) of Mn_2PtSn films measured at various temperatures 5 K, 10 K, 30 K, and 100 K with the magnetic field perpendicular to the film plane. The MR was derived using MR $= [\rho_{xx}(H) - \rho_{xx}(0)]/\rho_{xx}(0)$, where $\rho_{xx}(0)$ is the resistivity of the film at $H = 0$. The MR is negative at all measured temperatures and the magnitude is small (less than 1.0%) at 70 kOe. The MR curves exhibit the conventional behavior as found in most other ferromagnets. The slope of the MR(H) curves change abruptly near 30 kOe, which is more pronounced at low-temperature. If the spin structure is non-collinear as suggested by the saturation magnetization value, it may be that the 30 kOe field causes a change in the spin structure that is reflected in the electron scattering or seen in the magnetoresistance.

IV. CONCLUSIONS

In summary, the structural, magnetic, and electron-transport properties of Mn_2PtSn thin films have been investigated. Structural analysis shows that the crystal structure of the epitaxial Mn_2PtSn film is inverse tetragonal with lattice constants $a = b = 4.505$ Å and $c = 6.124$ Å (space group I-4m2, no 119). The measured saturation magnetization is 5.3 μ_B/f.u., which is smaller than the calculated value for ferromagnetic arrangement of Mn moments. The magnetization measurements revealed the bulk magnetocrystalline anisotropy constant K_v of about 11.3 Merg/cm^3 (1.13 MJ/m^3), with the easy axis in the plane of the film. The magnetoresistance ratio is 1.0% with the magnetic field applied perpendicular to the film plane. Perfect epitaxy on MgO suggests further study of these films in desire.

ACKNOWLEDGMENTS

This research was supported by NSF, DMR under Award No. DMREF: SusChEM 1436385. This work was performed in part in the Nebraska Nanoscale Facility, Nebraska Center for Materials and Nanoscience, which is supported by the National Science Foundation under Award No. ECCS: 1542182, and the Nebraska Research Initiative.

[1]A. D. Kent, B. Özyilmaz, and E. del Barco, "Spin-transfer-induced precessional magnetization reversal," Appl. Phys. Lett. **84**, 3897–3899 (2004).
[2]K. J. Lee, O. Redon, and B. Dieny, "Analytical investigation of spin-transfer dynamics using a perpendicular-to-plane polarizer," Appl. Phys. Lett. **86**, 022505 (2005).
[3]S. Mangin *et al.*, "Current-induced magnetization reversal in nanopillars with perpendicular anisotropy," Nat. Mater. **5**, 210–215 (2006).
[4]C. Chappert, A. Fert, and F. N. Van Dau, "The emergence of spin electronics in data storage," Nat. Mater. **6**, 813–823 (2007).
[5]S. S. P. Parkin, M. Hayashi, and L. Thomas, "Magnetic domain-wall racetrack memory," Science **320**, 190–194 (2008).
[6]J. Winterlik *et al.*, "Design scheme of new tetragonal Heusler compounds for spin-transfer torque applications and its experimental realization," Adv. Mater. **24**, 6283–6287 (2012).
[7]S. V. Faleev *et al.*, "Origin of the tetragonal ground state of Heusler compounds," Phys. Rev. Appl. **7**, 034022 (2017).
[8]S. Sanvito *et al.*, "Accelerated discovery of new magnets in the Heusler alloy family," Sci. Adv. **3**, e1602241 (2017).
[9]A. K. Nayak *et al.*, "Magnetic antiskyrmions above room temperature in tetragonal Heusler materials," Nature **548**, 561 (2017).
[10]Z. H. Liu *et al.*, "Giant topological Hall effect in tetragonal Heusler alloy Mn_2PtSn," Scr. Mater. **143**, 122–125 (2018).
[11]C. Phatak, O. Heinonen, M. De Graef, and A. Petford-Long, "Nanoscale skyrmions in a nonchiral metallic multiferroic: Ni_2MnGa," Nano Lett. **16**, 4141–4148 (2016).
[12]L. Wollmann, S. Chadov, J. Kübler, and C. Felser, "Magnetism in tetragonal manganese-rich Heusler compounds," Phys. Rev. B **92**, 064417 (2015).
[13]B. Balke, G. H. Fecher, J. Winterlik, and C. Felser, "Mn_3Ga, a compensated ferrimagnet with high Curie temperature and low magnetic moment for spin torque transfer applications," Appl. Phys. Lett. **90**, 152504 (2007).
[14]S. Ouardi *et al.*, "Stoichiometry dependent phase transition in Mn-Co-Ga-based thin films: From cubic in-plane, soft magnetized to tetragonal perpendicular, hard magnetized," Appl. Phys. Lett. **101**, 242406 (2012).
[15]H. Kurt *et al.*, "Magnetic and electronic properties of D022-Mn_3Ge (001) films," Appl. Phys. Lett. **101**, 132410 (2012).
[16]A. K. Nayak *et al.*, "Mn_2PtIn: A tetragonal Heusler compound with exchange bias behavior," Appl. Phys. Lett. **100**, 152404 (2012).
[17]V. Alijani *et al.*, "Increasing Curie temperature in tetragonal Mn_2RhSn Heusler compound through substitution of Rh by Co and Mn by Rh," J. Appl. Phys. **113**, 063904 (2013).
[18]B. Balke *et al.*, "Structural characterization of the Co_2FeZ (Z=Al, Si, Ga, and Ge) Heusler compounds by x-ray diffraction and extended x-ray absorption fine structure spectroscopy," Appl. Phys. Lett. **90**, 172501 (2007).
[19]Y. Huh *et al.*, "Magnetism and electron transport of MnyGa ($1 < y < 2$) nanostructures," J. Appl. Phys. **114**, 013906 (2013).

[20]O. Meshcheriakova *et al.*, "Large noncollinearity and spin reorientation in the novel Mn_2RhSn Heusler magnet," Phys. Rev. Lett. **113**, 087203 (2014).
[21]J. Kübler and C. Felser, "Berry curvature and the anomalous Hall effect in Heusler compounds," Phys. Rev. B **85**, 012405 (2012).
[22]Y. Huh *et al.*, "Effect of Co substitution on the magnetic and electron-transport properties of Mn_2PtSn," J. Phys.: Condens. Matter **27**, 076002 (2015).
[23]A. Nelson *et al.*, "Structural, magnetic, and electron transport properties of $Mn_{3-x}Pt_xSn$ (x = 0, 0.5, 1) nanomaterials," J. Appl. Phys. **115**, 17A923 (2014).
[24]G. Hadjipanayis, D. J. Sellmyer, and B. Brandt, "Rare-earth rich metallic glasses. 1. Magnetic hysteresis," Phys. Rev. B **23**, 3349–3354 (1981).
[25]Z. Wen, H. Sukegawa, S. Mitani, and K. Inomata, "Perpendicular magnetization of Co_2FeAl full-Heusler alloy films induced by MgO interface," Appl. Phys. Lett. **98**, 242507 (2011).
[26]Y. Tian, L. Ye, and X. Jin, "Proper scaling of the anomalous Hall effect," Phys. Rev. Lett. **103**, 087206 (2009).
[27]N. Nagaosa *et al.*, "Anomalous Hall effect," Rev. Mod. Phys. **82**, 1539–1592 (2010).